Volume 11
Number 22
14 June 2023
Pages 4823–5034

Journal of Materials Chemistry B

Materials for biology and medicine

rsc.li/materials-b

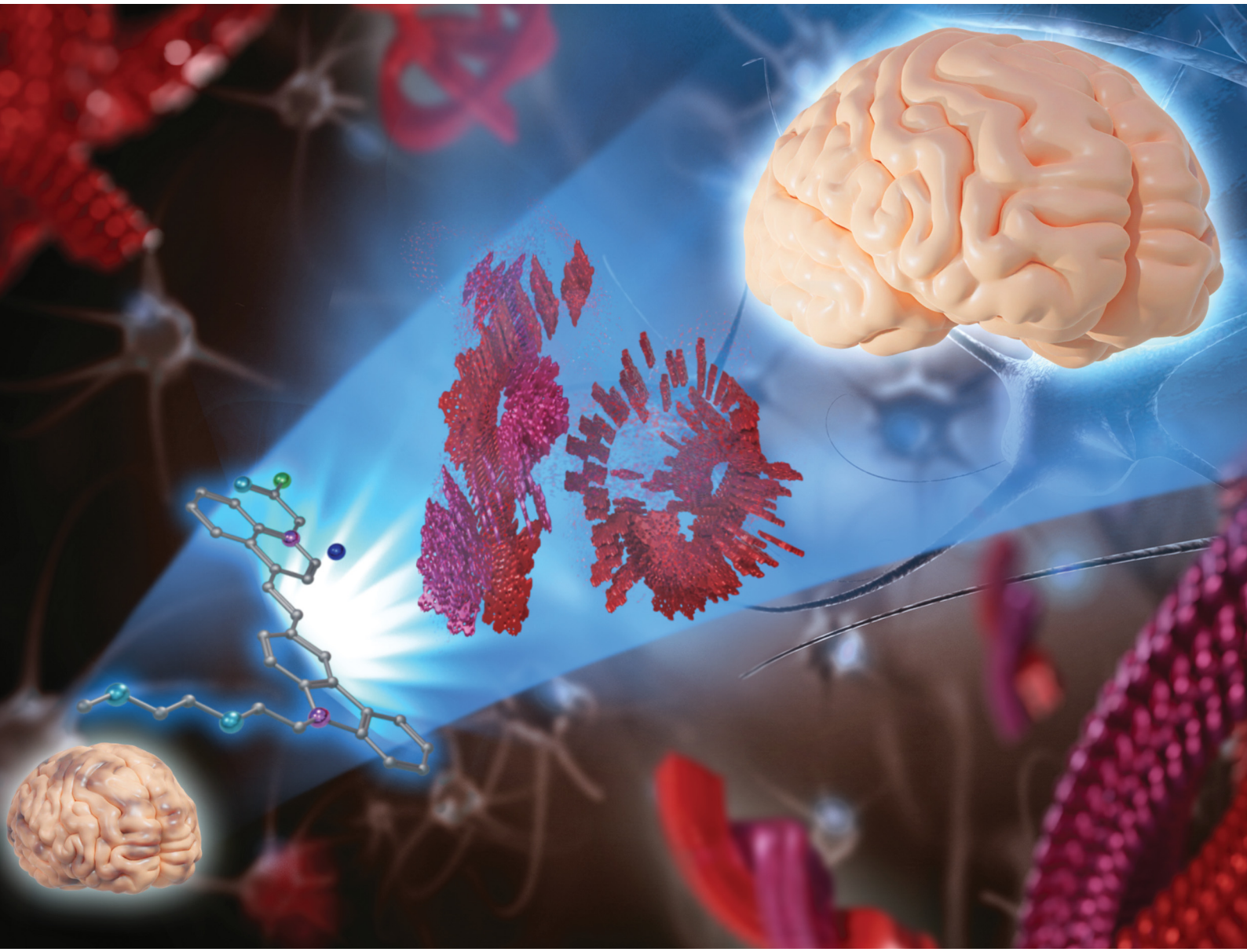

ISSN 2050-750X

ROYAL SOCIETY OF CHEMISTRY

PAPER

Guoli Song, Hung-Wing Li, Man Shing Wong *et al.*
Multifunctional theranostic carbazole-based cyanine for real-time imaging of amyloid-β and therapeutic treatment of multiple pathologies in Alzheimer's disease

10 YEARS ANNIVERSARY

Journal of Materials Chemistry B

ROYAL SOCIETY OF CHEMISTRY

PAPER

View Article Online
View Journal | View Issue

Cite this: J. Mater. Chem. B, 2023, 11, 4865

Multifunctional theranostic carbazole-based cyanine for real-time imaging of amyloid-β and therapeutic treatment of multiple pathologies in Alzheimer's disease†

Chen Chen, ‡[ab] Xueli Wang,‡[be] Di Xu,[b] Hailong Zhang,[b] Hei-Nga Chan,[b] Zhonghao Zhan,[a] Shizheng Jia,[a] Qingting Song,[d] Guoli Song, *[ac] Hung-Wing Li *[d] and Man Shing Wong *[b]

Received 14th January 2023,
Accepted 22nd April 2023

DOI: 10.1039/d3tb00082f

rsc.li/materials-b

Alzheimer's disease (AD) is a progressive and irreversible neurodegenerative disorder characterized by the synaptic and neuronal loss, which results in cognitive impairment in particular learning and memory. Currently, AD is incurable and no single confirmative test can clinically be used to diagnose AD. In light of the complex and multifactorial nature of AD etiology, the development of multifunctional/multi-target drugs that act on multiple pathological pathways and mechanisms shows great therapeutic potential for intervention of this devastating disease. We report herein a multifunctional theranostic cyanine, **SLCOOH**, which serves not only as a highly sensitive fluorescent probe for real-time imaging of amyloid-β (Aβ) contents in different age groups of transgenic (Tg) AD mice but also as an effective therapeutic agent for early AD intervention *via* multiple pathological targets in the AD mouse model. Remarkably, treatment with **SLCOOH** gives rise to multiple therapeutic benefits, including the amelioration of cognitive decline, a reduction in Aβ levels, a decrease in hyperphosphorylated tau proteins and tau depositions, and the alleviation of synaptic loss and dysfunctions in young triple Tg AD mice. Our results have demonstrated that in addition to superior Aβ imaging capability, **SLCOOH** exhibits versatile and effective multiple modes of drug action, signifying outstanding therapeutic potential to treat early onset AD. Our work also paves the way for the development of effective Aβ-targeted theranostic agents for AD.

Introduction

Alzheimer's disease (AD) is an irreversible, age-related, neurodegenerative disorder, which is characterized by progressive cognitive impairment and memory loss resulting from synaptic and neuronal loss.[1] Key pathological hallmarks of this disease are the deposition of senile plaques, which mainly consist of aggregated amyloid-β (Aβ) and the formation of neurofibrillary tangles, comprising mainly hyperphosphorylated microtubule-associated tau proteins in the brain.[2] Although current therapeutic drugs can provide symptomatic relief, they cannot modulate the underlying causes, thereby halting or reversing the disease progression, and thus offer no ultimate cure for AD.[3,4] In light of the multifactorial nature and complex pathology of AD, a more effective strategy has recently emerged to provide urgent disease-modifying treatment: the development of multi-target or multifunctional drugs, in which a single molecule or entity simultaneously acts on more than one specific etiological target of AD, such as the prevention of Aβ aggregation and deposition, the alleviation of tau hyperphosphorylation, the amelioration of synaptic deficits, or the prevention of neuronal loss.[5,6] Compounds that show multi-targeting properties for AD are rather rare. One common design approach to develop multi-target drugs is to integrate multiple functional structural units that target multiple causes of AD

[a] Shenzhen Key Laboratory of Marine Bioresources and Ecology, College of Life Sciences and Oceanography, Shenzhen University, Shenzhen, China. E-mail: lilys@szu.edu.cn
[b] Department of Chemistry, Hong Kong Baptist University, Kowloon Tong, Hong Kong, SAR China. E-mail: mswong@hkbu.edu.hk
[c] Shenzhen Bay Laboratory, Shenzhen, China
[d] Department of Chemistry, Chinese University of Hong Kong, Shatin, Hong Kong, SAR China. E-mail: hungwingli@cuhk.edu.hk
[e] Present address: College of Pharmaceutical Sciences, Hebei University, Baoding, 071002, China

† Electronic supplementary information (ESI) available: Detailed synthetic and experimental procedures, photophysical properties, selectivity study, fluorescence titration plots, results of displacement assay and ThT fluorescence assay, MTT assays, neuroprotection and ROS inhibition studies, LC-ESI-MS spectra of brain extracts of the **SLCOOH**-treated mice, *ex vivo* images of brain slices, results of Western blot analyses and spectra for compound characterization. See DOI: https://doi.org/10.1039/d3tb00082f

‡ Chen Chen and Xueli Wang contributed equally.

into a single entity. Nevertheless, multi-target drugs that show effective *in vivo* efficacy are limited due to a lack of such a strategy in practice.[7–11]

It is widely believed that aggregation of Aβ peptides being an early causative factor and event in the pathogenesis of AD is caused by an imbalance between the production and clearance of Aβ peptides.[12] An agent simply showing an inhibitory effect against Aβ aggregation does not offer a disease-modifying remedy for AD.[13] However, the ability to modulate the over-production and/or impaired clearance of Aβ is one of the primary therapeutic goals in the development of treatment agents for AD.

Synaptic deficits caused by the loss of dendritic spines, a decrease in the number and/or density of synapses, and the impairment of synaptic plasticity are believed to be closely related to cognitive decline in patients with AD.[14] Studies have shown that both Aβ and tau pathology-induced aberrant calcium (Ca^{2+})-dependent synaptic transmission underlie synaptic depression. Numerous studies have also shown that the ability to enhance Ca^{2+}/calmodulin-dependent protein kinase II (CaMKII) signalling could reduce synaptic dysfunction and thus improve cognitive function.[15] Furthermore, previous studies have demonstrated that synaptic dysfunction can be induced by the excess release of the excitatory neurotransmitter glutamate, which causes an over-activation of NMDARs.[16,17] Over-stimulation of NMDARs leads to excessive influx of Ca^{2+}, resulting in excitotoxicity and ultimately neuronal cell death in patients with AD.[18] Therefore, the development of an effective NMDAR antagonist would be an attractive strategy to prevent synaptic dysfunction in patients with AD.

Over the years, various smart fluorescent probes have been developed for selective detection and imaging of Aβ plaques.[17–23] Carbazole-based cyanine is an intriguing class of multifunctional fluorophores for AD as it exhibits not only desirable *in vivo* and *ex vivo* imaging properties for Aβ species, but also attractive *in vivo* therapeutic potential for the treatment of AD.[24–27] Importantly, its molecular and biological properties can easily be tuned by modifying the R substituent on the quinolinium ring (Fig. 1A). Cyanine SLOH with R = CH_2CH_2OH[28] and SLM with R = CH_3[29] were shown to exhibit different degrees of inhibition against Aβ aggregation *in vitro*, low cytotoxicity toward SH-SY5Y cells, and *in vivo* therapeutic effects in an AD-affected mouse, signifying the promising potential of this class of molecules as theranostic agents for AD. In the search for an effective multi-targeted cyanine with multiple therapeutic benefits for the pre-symptomatic intervention of AD prior to irreversible alteration, an extensive structural modification of the lead cyanine molecule has been performed and tested.

The present study reports a newly developed multifunctional theranostic cyanine, **SLCOOH** with R = CH_2COOH (Fig. 1A), which has been shown to serve as not only a highly sensitive fluorescent probe for the real-time detection and monitoring of Aβ contents, but also an effective multi-targeted therapeutic agent to treat multiple AD-related pathologies in AD-affected mice. **SLCOOH** exhibited a very strong Aβ-selective binding fluorescence enhancement (160–265 fold increase) concomitant with a blue shift of the emission spectrum (Fig. 1B and Fig. S1C, ESI†), indicating a strong interaction between Aβ and **SLCOOH**. Because of its good solubility, strong binding affinity and high selectivity toward Aβ, and good blood-brain barrier (BBB) permeability, **SLCOOH** was found to be practically useful and sensitive as a fluorescent probe for real-time imaging of Aβ contents in different age groups of transgenic (Tg) AD mice. In addition to having superior biocompatibility with a very low cytotoxicity ($LC_{50} > 200$ μM) and acute toxicity at $LD_{50} > 125$ mg/kg (*via* a tail-vein injection) as compared to other cyanines, **SLCOOH** was found to suppress Aβ aggregation (Fig. S3, ESI†), exhibit a neuroprotective effect against Aβ-induced toxicity (Fig. S4, ESI†), and inhibit Aβ-induced ROS production (Fig. 1C), suggesting its potential for therapeutic intervention of AD. Remarkably, administration of 4-month old AD mice with **SLCOOH** for 2 months improved neurological functions, effectively ameliorating cognitive impairment concomitant with an alleviation of Aβ and tau pathologies. Furthermore, **SLCOOH** reversed synaptic loss and synaptic dysfunction in AD mice by activating the Ca^{2+}-dependent signalling pathway and modulating the balance of NMDARs, resulting in a reduced load of intercellular Ca^{2+}. The results of the present study demonstrate for the first time that **SLCOOH** exhibits the most potent multiple modes of drug action by targeting multiple pathological pathways to intervene in the early onset of AD, highlighting the tremendous therapeutic potential for AD.

Results and discussion

The synthetic route for the preparation of **SLCOOH** is outlined in Scheme S1 (ESI†), and the condensation of lepidine and the corresponding carbazole-carbaldehyde was the key step in the construction of the cyanine skeleton. This new cyanine was fully characterized by ^{1}H NMR, ^{13}C NMR, and HRMS, and its structure was found to align with the corresponding spectroscopic data. **SLCOOH** exhibited a strong absorption peak at 469 nm and a weak emission at 666 nm with a fluorescence quantum yield (Φ_{PL}) of 0.003 in PB (Fig. S1A, ESI†). As anticipated, **SLCOOH** showed high selectivity toward Aβ (Fig. S1B, ESI†) and strong fluorescence turn-on concomitant with a blue-shift in emission upon titration with Aβ species (160–265 fold enhancement with $Aβ_{1–42}$) and a low limit of detection (LOD) toward Aβ species (0.52–1.62 μM) (Fig. S1F and Table S2, ESI†), implicating its potential use as an effective fluorescence probe for *in vivo* Aβ imaging. The binding dissociations (K_d) of **SLCOOH** and Aβ species were estimated by a saturation assay, which were found to be in the range of 26–66 μM (Fig. S1E and Table S2, ESI†). The displacement assay[30] of Thioflavin T (ThT) bound $Aβ_{1–42}$ fibrils with **SLCOOH** was also performed in which **SLCOOH** effectively displaced ThT from the ThT/$Aβ_{1–42}$ aggregate complex and the K_d of **SLCOOH** and Aβ fibrils was determined to be 2.31 ± 55 μM (Fig. S1G, ESI†). All these results confirmed that **SLCOOH** strongly and selectively interacts with Aβ, giving rise to the possibility of suppressing Aβ aggregation, as evidenced by the ThT fluorescence assay of $Aβ_{1–42}$ in the

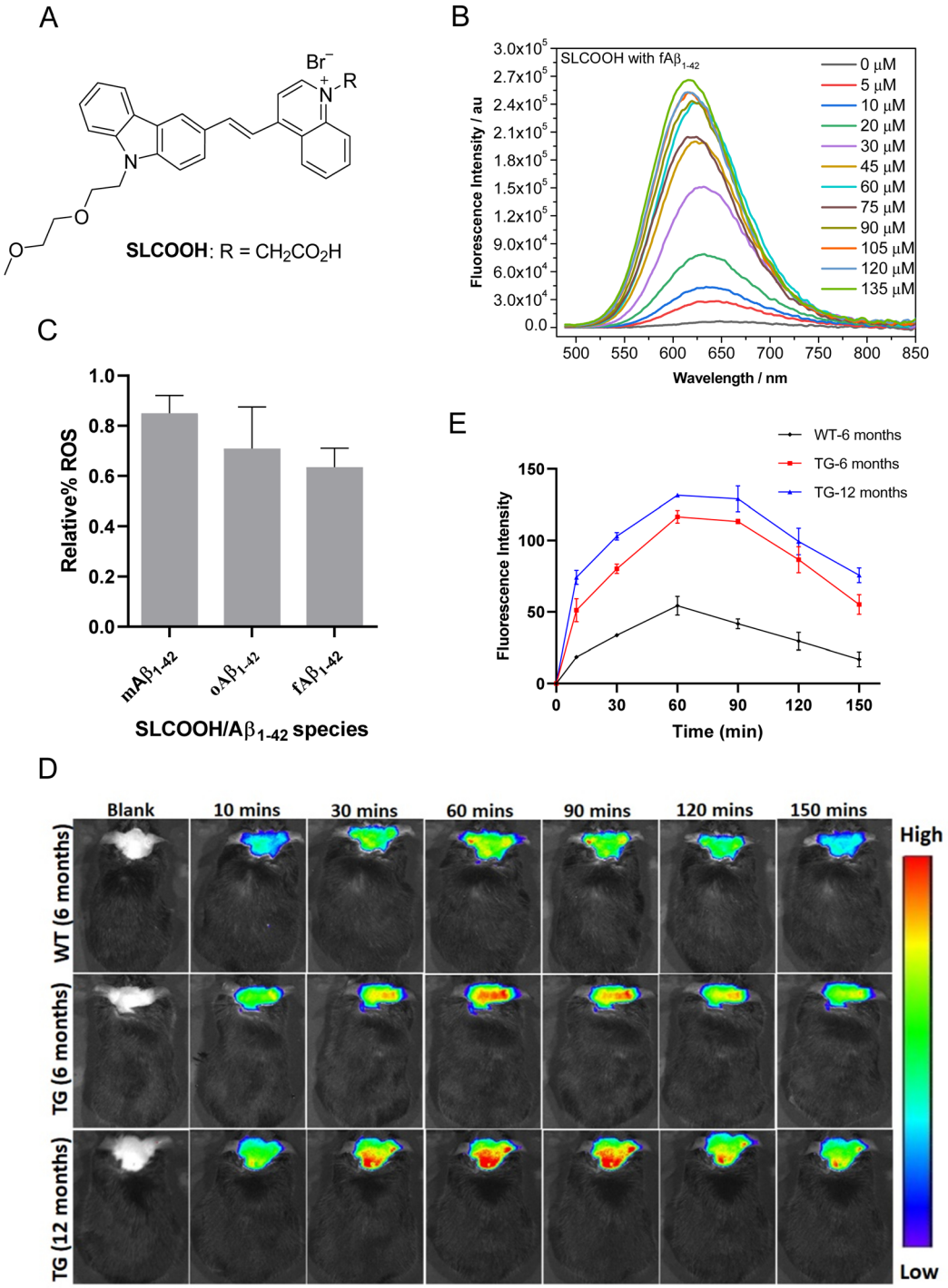

Fig. 1 (A) Chemical structure of carbazole-based cyanine, **SLCOOH**. (B) Fluorescence spectra of **SLCOOH** upon titrating against various concentrations of $A\beta_{1-42}$ fibril. (C) Plots of the relative ROS level against $A\beta_{1-42}$ monomesr, oligomers and fibril-induced cytotoxicity toward SH-SY5Y neuronal cells by **SLCOOH**. (D) *In vivo* fluorescence brain imaging of 6- and 12-month-old 5XFAD Tg mice and a wild-type (WT) mouse. All the mice were injected with the **SLCOOH** (100 μL 10 mg kg^{-1}) in PB (0.5 M, pH = 7.4) and 10% DMSO *via* tail vein and their fluorescence signals were monitored in real-time over a period of 150 min with λ_{ex} = 465 nm and λ_{em} = 575–650 nm. (E) Plot of the relative fluorescence intensity of **SLCOOH** with the respective mice at difference time points.

presence of **SLCOOH** (Fig. S2, ESI†). The blue-shift in emission of the relatively planar **SLCOOH** upon binding with Aβ implicates that **SLCOOH** resides in a hydrophobic environment of Aβ fibrils/plaques interacting with β-sheet conformed Aβ *via* the π–π stacking interactions.[24]

The viability of human neuroblastoma SH-SY5Y cells was quantitatively evaluated using the 3-(4,5-dimethylthiazol-2-yl)-diphenyltetrazolium bromide (MTT) method. The MTT assay indicated that **SLCOOH** was negligibly toxic to neuronal cells with LC_{50} > 200 μM (Fig. S3, ESI†). The acute toxicity was also

very low (LD_{50} > 125 mg kg^{-1} *via* a tail-vein injection), demonstrating that **SLCOOH** is highly biocompatible for bioapplications. Intriguingly, **SLCOOH** exhibited a neuroprotective effect against Aβ species toward SH-SY5Y neuronal cells (Fig. S4, ESI†), and effectively alleviated Aβ-induced ROS production (Fig. 1C), indicating its potential for therapeutic intervention in Aβ pathology.

To be useful in practice as a diagnostic and/or therapeutic agent for AD, good BBB permeability is indispensable. To probe the BBB penetrability of **SLCOOH**, brain extracts from the **SLCOOH**-treated mice were analyzed by liquid chromatography-electrospray ionization-mass spectrometry (LC-ESI-MS) from which a strong $[M + 1]^+$ peak with *m*/*z* of 482.3336 was observed in the mass spectrum (Fig. S5, ESI†) suggesting the presence of intact **SLCOOH** in the brain, and therefore its BBB permeability. Then, *in vivo* fluorescence brain imaging of different age groups (6 and 12 months old) of 5XFAD Tg mice and a wild-type (WT) mouse after a tail vein injection with **SLCOOH** was performed. Unambiguously, strong fluorescence signals of **SLCOOH** were clearly observed in all the tested mice over a period of 150 min (Fig. 1D), in which the fluorescence intensity reached a maximum approximately one hour after the injection (Fig. 1E), further affirming the BBB penetrability of SLOOH. It is worth mentioning that the older Tg mice exhibited stronger fluorescence signals than the younger Tg and WT mice at each time point. The stronger fluorescence exhibited in the older Tg mice compared to those of the younger and WT counterparts is attributed to the increased number of Aβ plaques in the older Tg and the enhanced fluorescence of **SLCOOH**, induced by the binding of Aβ plaques. Besides, the malfunctioning of the BBB in Tg mice might contribute stronger fluorescence signals in Tg mice than in WT mice. Furthermore, the ability of

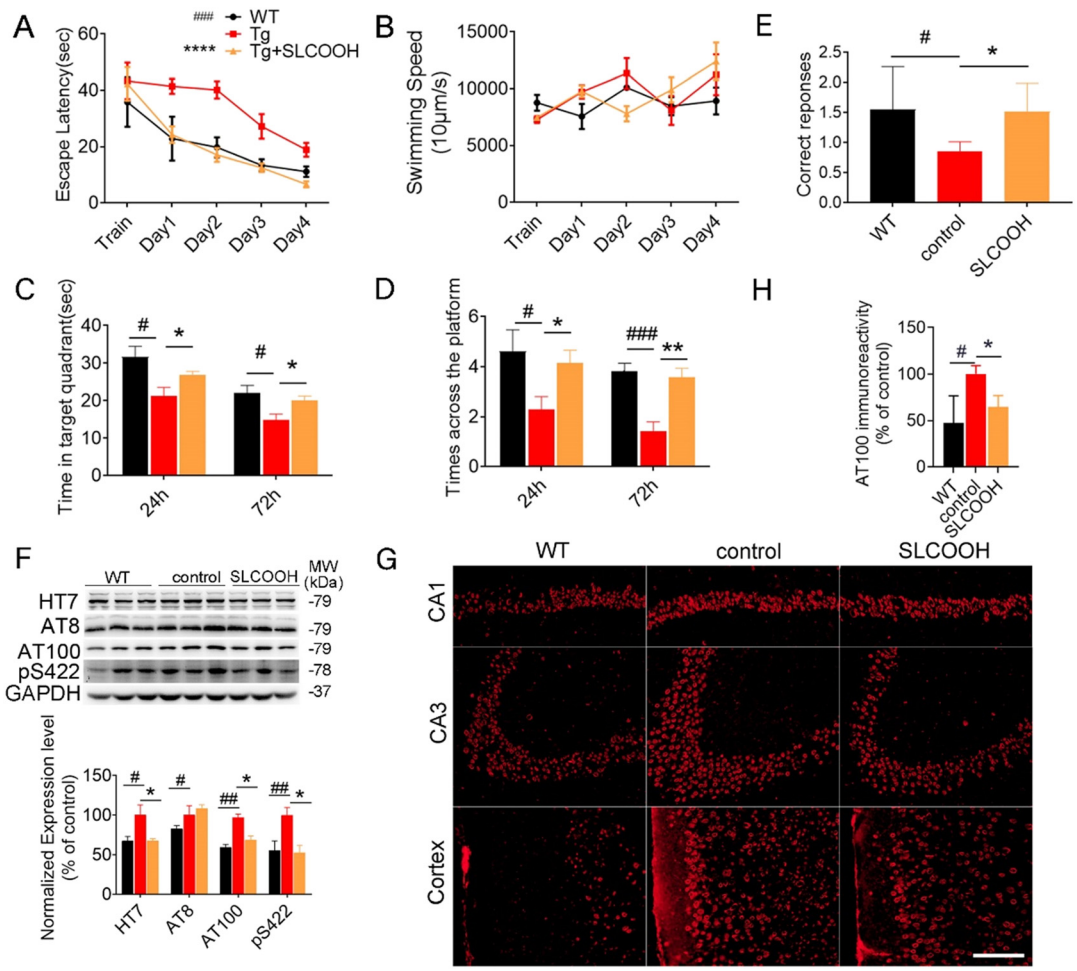

Fig. 2 (A) In learning trials, mice were tested for 4 days and the escape latency of each mouse was recorded. (two-way analysis of variance, #$p < 0.01$, AD *vs.* WT mice; *$p < 0.01$, **SLCOOH**-treated *vs.* AD mice, $n = 19$). (B) The average swimming speed of mice in each group. (C and D) In the probe trial of 24 h and 72 h, the time that mice swam to the target quadrant where the hidden platform was previously placed and the number of times that mice across the platform location are shown. #$p < 0.05$; ###$p < 0.001$, AD *vs.* WT mice; *$p < 0.05$; **$p < 0.01$, **SLCOOH**-treated *vs.* AD mice, $n = 19$. (E) Correct response in a T-maze test performed with 6-month-old WT, AD and **SLCOOH**-treated mice (means ± SEMs) (#$p < 0.05$, *vs.* WT mice; *$p < 0.05$, *vs.* AD mice. $N = 10$ mice). (F) Representative western blot images of HT7, AT8 (Ser202), AT100 (Ser214, Thr212), pS422 (Ser422) expression levels in cortex. The densitometry results were normalized against levels of GAPDH and their respective western blot analysis (#$p < 0.05$, ###$p < 0.01$, *$p < 0.05$, $n = 6$). (G and H) Immunofluorescence staining of AT100 in the hippocampus (CA1, and CA3) and cortex of mice and immunofluorescence analyses of the stained fluorescence. (#$p < 0.05$, *$p < 0.05$, $n = 3$ (2 slices per mouse)) CA1, cornu ammonis 1; CA3, cornu ammonis 3. Scale bar: 20 μm.

SLCOOH to target Aβ in the brain of the 5XFAD Tg mice was investigated by *ex vivo* co-staining studies with Aβ plaque-specific staining dye, thioflavin-S (ThS), and Aβ antibodies (6E10 or 4G8), which detect all Aβ species and amyloid precursor proteins (APP). In contrast to the absence of stained clusters in the brain slices of the age-matched WT mice (Fig. S6B, ESI†), the red fluorescence clusters colocalized well with the green fluorescence of ThS, as well as 6E10 and 4G8 antibodies, in brain slices of the 6-month-old AD mice (Fig. S6A, ESI†), confirming the Aβ-targeting capability of **SLCOOH**.

To evaluate the efficacy of **SLCOOH** for treatment against cognitive deficits, learning and memory were assessed in the 4-month-old triple transgenic (3XTg)-AD mice, which were treated with **SLCOOH** for 2 months, using the Morris water maze and T-maze tests. As shown in Fig. 2A, the escape latencies of the AD mice were significantly longer than those of the WT mice ($\#p < 0.05$, $n = 10$), while **SLCOOH**-treated AD mice showed marked improvement in their total escape latencies in the 5 days hidden platform test ($*p < 0.05$, $n = 19$). Furthermore, although the AD group spent significantly less time in the target quadrant than the control group ($\#p < 0.05$; Fig. 2C), the **SLCOOH**-treated AD mice spent longer in the target quadrant ($**p < 0.01$; Fig. 2C) and traveled more frequently across the platform ($*p < 0.05$; Fig. 2D) compared to the AD control group in the probe trials. In the T-maze experiment, the number of AD mice entering the correct arm was significantly lower than that of WT mice. In contrast, treatment with **SLCOOH** significantly increased the percentage of correct choices in the AD mice ($*p < 0.05$; Fig. 2E). Consistently, both tests unanimously demonstrated a significant improvement in the learning and memory abilities of the **SLCOOH**-treated AD mice compared to those of the controls. As Aβ aggregation is an early feature of AD pathology and Aβ oligomers are more neurotoxic, the Aβ oligomer levels with molecular weights of 40 and 20 kD in the brains of the investigated mice were assessed and compared using western blot analysis. Despite a marked increase in the Aβ oligomer levels in the AD mice, the levels were significantly reduced in the hippocampi of the treated AD mice (Fig. S7, ESI†). In addition, treatment with **SLCOOH** significantly reduced the tau (HT7) and phosphorylated tau [AT8 (Ser202), AT100 (Ser214, Thr212), pS422 (Ser422)] content in the brains of AD mice, although the mice developed noticeably higher expression levels of tau than the WT mice (Fig. 2F). As depicted in Fig. 2G, such a reduction in phosphorylated tau levels could also be visualized by immunofluorescence staining of AT100 antibodies in the brain slices of the investigated mice, and was attributed to a substantial decrease in the activity of glycogen synthase kinase-3β (GSK3β) in the treated mice. In the AD mice, p-GSK3β (Ser9) expression was found to be significantly lower than in the WT mice; however, it was remarkably increased after treatment with **SLCOOH**. On the other hand, there were no obvious changes in PP2A levels in the brain after treatment (Fig. S8, ESI†). The ubiquitin proteasome system (UPS) and autophagy–lysosomal pathway are two primary mechanisms which degrade abnormal or misfolded proteins in cells; however, the reduction of Aβ and tau expression in the **SLCOOH**-treated mice was found to be due to the activation of clearance by upregulating the autophagic pathway, as revealed by the expression level of an autophagy biomarker, light chain protein 3 (LC3). In the autophagy-lysosomal pathway, the inactive LC3-I form is converted to an active LC3-II form during the formation of autophagosomes. It was found that the LC3-II/LC3-I level was significantly higher in the hippocampi of AD mice as compared to WT mice, and **SLCOOH** treatment further increased the LC3-II/LC3-I ratio. On the other hand, the levels of ubiquitinated proteins did not vary between the tested groups (Fig. S9, ESI†). To further confirm the modulation of the autophagic pathway after treatment with **SLCOOH**, the expression levels of various signaling proteins, including p-mTOR/mTOR, p-p70S6K/p70S6K, beclin 1, p62, and cathepsin D, using western blot analyses were also investigated, the results of which consistently support the activation of the pathway (Fig. S10, ESI†).

Normal synaptic structures and function are essential for maintaining cognitive function. To assess the effect of **SLCOOH** on the synaptic structure of the **SLCOOH**-treated AD mice, a transmission electron microscopic study was performed to image hippocampal and cortical synapses. As shown in Fig. 3A and B, there was an increase in the number of synapses in the treated mice as compared to those of the AD control group. Western blot analysis consistently showed that both postsynaptic density protein 95 (PSD-95) and synaptophysin were increased in the brains of **SLCOOH**-treated mice relative to those of the controls (Fig. S11, ESI†). Furthermore, despite the reduction in the number of dendritic spines in AD mice, which are responsible for excitatory neurotransmission in neurons, there was a significant increase in the number of dendritic spines in the brains of the **SLCOOH**-treated AD mice (Fig. 3C). All these findings collectively support the beneficial effect of treatment with **SLCOOH** on restoring synaptic structures in AD brains. Remarkably, in regard to the synaptic function, **SLCOOH** treatment also significantly enhanced hippocampal potentiation of the CA1-Schaffer collateral pathway, as indicated from the measured slope of the field excitatory postsynaptic potential (fEPSP) of the treated mice, as shown in Fig. 3D. This suggests an improvement in the synaptic plasticity in the **SLCOOH**-treated AD mice, which was attributed to the activation of the CaMKII/Erk/CREB postsynaptic signalling pathway, as revealed by western blot analysis of the corresponding protein kinase expression levels (Fig. S12, ESI†). On the other hand, the impairment of synaptic plasticity could be induced by intracellular Ca^{2+} overload in patients with AD. As the entry of Ca^{2+} is mainly regulated by the NMDARs on the synaptic membrane, the expression levels of the NMDAR regulatory subunits, synaptic NMDAR2A, and extrasynaptic NMDAR2B were investigated.[31–33] Interestingly, **SLCOOH** was able to regulate Ca^{2+} influx into primary neurons (Fig. S13, ESI†). Furthermore, the results of an assessment of the expression levels of the regulatory subunits of NMDAR2 in the brains of the tested groups showed that despite the significantly higher level of extrasynaptic NMDAR2B and phosphorylated

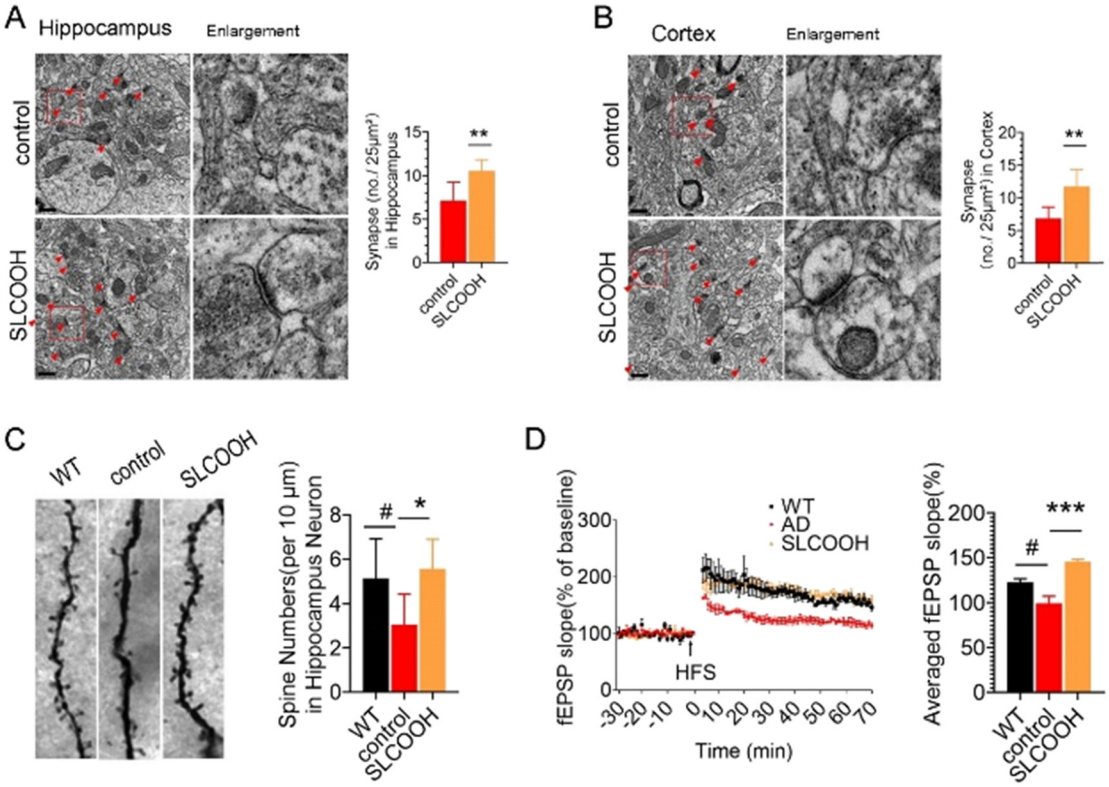

Fig. 3 TEM images of synapses in the (A) hippocampus and (B) cortex of the control and **SLCOOH**-treated mice. The synapses are pointed by the arrows (scale bar: 0.5 μm) and their respective quantification of synapses in the hippocampus and cortex (**$p < 0.01$, $n = 3$ (2 slices per mouse)). (C) Representative images and their respective quantification of the dendritic spines in the hippocampus in 6-month-old mice by Golgi staining (#$p < 0.05$, *$p < 0.01$. $n = 3$ (2 slices per mouse), Scale bar: 2 μm. (D) Slope of the field excitatory postsynaptic potential (fEPSP) in response to 100 HZ stimulation in the Schaffer collateral CA1-region of WT, AD and **SLCOOH** mice and their respective quantification of the averaged fEPSP slope of (D) (means ± SEMs) (#$p < 0.05$, ***$p < 0.001$. $n = 6$).

NMDAR2B (p-NMDAR2B) in the hippocampi of AD mice than in WT mice, these levels were greatly reduced after **SLCOOH** treatment (Fig. S14, ESI†), indicating that the Ca^{2+} influx was downregulated. All these findings suggest that **SLCOOH** can reduce synaptic dysfunction in AD mice.

Experimental

Animal care and treatment

We purchased 3xTg-AD (homozygous mutant APP_{SWE}, $PS1_{M146V}$, and Tau_{P301L}) mice and their background strain, and wild-type (WT, C57BL/6/129S) mice from the Jackson Laboratory (USA). The animals were housed in individual ventilated cages categorised into group at a room temperature of 23 ± 1 °C and a 12/12 h reversed light/dark cycle. Food and water were provided at will 4-month-old 3xTg-AD mice ($n = 19$; 9 males and 10 females) were treated with **SLCOOH** (4.5 mg kg^{-1} day^{-1}) *via* intraperitoneal injection for 60 days. Control AD mice ($n = 19$; 10 males and 9 females) were treated with 0.1 M phosphate buffer saline at pH 7.2. The experiments and procedures were performed in strict accordance with the institutional guidelines regarding experimental animal use at Shenzhen University. The protocol was approved by the Animal Ethical and Welfare Committee of Shenzhen University (Permit Number: AEWC-20140615-002). All efforts were made to minimize animal suffering.

Behavioural examination

Morris water maze test (MWM). The MWM test included 1 day of visible platform training and 5 days of hidden platform tests, as well as two probe trials taken at 24 h and 72 h after the last hidden platform test. In visible platform training, mice were given 60 s to find the platform from each quadrant. In learning trails, mice underwent four trials of swimming from each quadrant, with inter-trial intervals of 1 h. After the learning trails, probe trials were performed in which the platform was removed. Automated video tracking recorded the behaviours of mice including swimming speed, escape latency in the hidden platform test, and the counts of passage through the location of the original platform, and time spent in the platform quadrant in the probe test. The data were analyzed by two-way analysis of variance.

T maze test. The T-maze is classically used to assess the working memory and reference memory studies in rodents. The T-maze apparatus comprised a start arm and two goal arms (30 × 6 × 15 cm). Mice were food-deprived by receiving only 50% of the standard daily food intake for three days and were then trained simultaneously on 3 consecutive days. On each training day, food was placed in a set arm (goal arm), and all mice were placed in the start arm for approximately 3 min to allow free exploration of the food. After the three training sessions, the food was removed from the target arm, and each

mouse was given 3 min in the start arm. In the test, the latency to reach the goal arm and the number of correct and incorrect entries were recorded. In between trials, the arms of the apparatus were wiped with alcohol to remove any olfactory cues.

SDS-PAGE and western blot analysis

After behavioural assessment, the animals were euthanized and their brains were rapidly isolated. The left hemispheres were fixed in 4% paraformaldehyde and stored for further immunohistochemical and immunofluorescent analyses. The hippocampus and cortex samples were dissected from the right hemispheres and expression levels of proteins in these two regions were then analyzed by western blot. As an internal control, α-tubulin, GAPDH or β-actin was used to normalize protein loading (Proteintech, USA). Finally, protein blots were developed using the enhanced chemiluminescence kit (Thermo Scientific SuperSignal, USA) and measured using a Tanon 5200 (Tanon, Shanghai, China). The total densities of protein bands were recorded and analyzed using the image analysis tool (ImageJ software).

Immunofluorescence staining. Left hemispheres were embedded and frozen in an optimal cutting temperature compound, and then sectioned (20 μm thickness) with a Leica Cryostat. Slices were permeabilized with 0.2% Triton X-100 for 20 min at room temperature (RT), incubated with blocking solution (10% goat serum in PBS) for 10 min, and then incubated with primary antibody (1 : 150 diluted in blocking buffer, anti-AT100, Thermo Scientific) overnight at 4 °C. Slices were then washed thrice with 1× PBS and incubated with a fluorescence-labelled secondary antibody (1 : 500 diluted in blocking buffer, Abcam) for 2 h at RT in darkness. Slices were washed an additional three times with 1× PBS. Finally, sections were imaged by fluorescence microscopy (Zeiss, Germany). Three sections of each animal were assessed.

Transmission electron microscopy

TEM was performed as previously described.[34] Briefly, mouse cortexes and hippocampi were fixed with 2.5% glutaraldehyde and 1% osmium tetroxide for 2 h at 4 °C, dehydrated in a series of graded ethanol, and embedded in epoxy resin. Then, samples were sectioned into ultrathin slices (DiATOME knife and Leica ultramicrotome), stained with 2% uranyl acetate and 2% lead citrate. Images were acquired using a Tecnai G2 Spirit transmission electron microscope (FEI, USA).

Golgi staining

Golgi-Cox staining was performed with a FD Rapid Golgi Stain kit (FD NeuroTechnologies, USA). Briefly, freshly harvested brain tissues from 6-month-old mice were rinsed with double distilled water and were then immersed in 10 mL of impregnation solution (a mixture of equal volumes of Solutions A and B mixed 24 h prior to removal of the precipitates) for 2 weeks at room temperature. Subsequently, tissues were transferred to Solution C for 72 h in the dark. Then, coronal sections of 150 μm thickness were cut with a vibratome (Leica VT 1000S), placed in the dark and allowed to dry at room temperature overnight. After staining with Solutions D + E and dehydration in a gradient ethanol series, slides were covered with permount TM mounting medium and imaged with a fluorescence microscope (Olympus, BX51).

Electrophysiological analysis

Brains were quickly isolated after mice were euthanized and placed into ice-cold artificial cerebrospinal fluid (ACSF) continuously bubbled with carbogen (95% O_2/5% CO_2) containing 119 mM sucrose, 2.5 mM KCl, 2.5 mM $CaCl_2{\cdot}2H_2O$, 26.2 mM $NaHCO_3$, 1.0 mM $NaH_2PO_4{\cdot}2H_2O$, 1.3 mM $MgCl_2{\cdot}6H_2O$ and 11.0 mM glucose, then cut into 300 μm slices on a vibrating blade microtome (Leica VT1200). Slices were transferred to a holding chamber at 32 °C for 2 h in ACSF with carbogen. fEPSP values were recorded using a MED64 multichannel recording system (Alpha Med Systems, Osaka, Japan; array size: 1 × 1 mm; each electrode: 50 × 50 μm; interpolar distance: 150 μm; electrode array: 8 × 8). For each slice, the baseline stimulus intensity was set at −10 μA every 20 s for 30 min. LTP was induced with a conditioning stimulus consisting of three theta burst trains (ten 5 Hz series of four 100 Hz pulses each, 40 s apart). More than nine slices from 3–4 mice per condition were used.

Primary cell culture and calcium imaging

Primary neurons were isolated from the cortexes of postnatal day 1 3xTg-AD mice. Meninges-free cortexes were collected and dissociated into 1 mm^3 fragments on ice. Fragments were digested in papain solution (2 mg mL^{-1}) in dish for 30 min at 37 °C, then gently rinsed twice in Dulbecco's Modified Eagle Medium with 10% FBS to inactive papain; 3 mL of Opti-MEM (supplemented with 2% B27 and 1% penicillin–streptomycin) was added and the suspension was gently pipetted up and down <10 times. After incubation for 3 min, the supernatant containing separated neurons was collected. This process was repeated twice. The collected neurons were diluted to a density of 105–106 mL^{-1} and seeded in 6-well plates, then cultured in a humidified incubator with 5% CO_2 at 37 °C for 9 days. Cells were transfected with AAV9-jRCaMP1 (Gibco) for 24 h. After transfection, 10 μM **SLCOOH** was added to the medium for 4 h, followed by fixing with 4% PFA after washing with PBS, and then were observed and photographed under a laser confocal microscope (Olympus, Japan).

Statistics

All results are shown as mean ± standard error of the mean and analyzed by analysis of variance or *t*-test. Differences were considered statistically significant when p-values were < 0.05.

In vivo and *ex vivo* imaging of SLCOOH in mouse models

The previously adopted imaging and co-staining procedures[34] were followed in which the mice were anesthetized under the same conditions, kept still, and then injected with 100 μL of **SLCOOH** (10 mg kg^{-1}) through the tail vein.

Conclusions

In conclusion, the results of the present study have demonstrated that the nontoxic and biocompatible cyanine **SLCOOH**

is a highly sensitive and effective probe for the *in vivo* and *ex vivo* detection and visualization of Aβ contents in different age groups of transgenic AD mice. Furthermore, treatment with **SLCOOH** in young triple transgenic AD mice simultaneously mitigates cognitive impairment, alleviates Aβ and tau neuropathologies by activating the autophagy pathway, and ameliorates synaptic loss and dysfunction by restoring synaptic structures, regulates the Ca^{2+}-dependent CaMKII/CREB signalling pathway, and inhibits extrasynaptic NMDARs *via* modulation of intercellular Ca^{2+} ion overloading, offering multiple effective therapeutic benefits in AD mouse models. For the first time, the multifunctional theranostic cyanine **SLCOOH**, capable of imaging of Aβ contents *in vivo* and targeting multiple pathological pathways or mechanisms of neurodegeneration, was unambiguously demonstrated, highlighting the tremendous therapeutic potential to treat early onset AD. Our work provides a successful example of a multi-target/multifunctional drug acting on multiple etiological targets to intervene in the early onset of AD, which opens up an alternative avenue for the development of Aβ-targeted theranostic agents for AD.

Conflicts of interest

There are no conflicts to declare.

Acknowledgements

This work was supported by the Collaborative Research Fund (C2012-15G) and General Research Fund (12302620 and 12302021) of Hong Kong Research Grant Council, the National Natural Science Foundation of China (No. 21675135 and 31800681), the Interdisciplinary Research Clusters Matching Scheme, Research Committee of Hong Kong Baptist University (IRCMS/19-20/H02), the Guangdong Natural Science Foundation for Major Cultivation Project (2018B030336001), and the Shenzhen-Hong Kong Institute of Brain Science-Shenzhen Fundamental Research Institutions (No. 2019SHIBS0003). HWL is grateful for the support of the Direct Grant from the Chinese University of Hong Kong. The authors are also grateful to Prof. Min Li and Dr Ashok Iyaswamy for providing 5XFAD transgenic mice for the fluorescence imaging experiments at the School of Chinese Medicine, Hong Kong Baptist University.

Notes and references

1 G. B. Stokin, C. Lillo, T. L. Falzone, R. G. Brusch, E. Rockenstein, S. L. Mount, R. Raman, P. Davies, E. Masliah, D. S. Williams and L. S. Goldstein, *Science*, 2005, **307**, 1282–1288.
2 C. Ballatore, V. M. Lee and J. Q. Trojanowski, *Nat. Rev. Neurosci.*, 2007, **8**, 663–672.
3 D. Olivares, V. K. Deshpande, Y. Shi, D. K. Lahiri, N. H. Greig, J. T. Rogers and X. Huang, *Curr. Alzheimer Res.*, 2012, **9**, 746–758.
4 M. B. Colovic, D. Z. Krstic, T. D. Lazarevic-Pasti, A. M. Bondzic and V. M. Vasic, *Curr. Neuropharmacol.*, 2013, **11**, 315–335.
5 O. Benek, J. Korabecny and O. Soukup, *Trends Pharmacol. Sci.*, 2020, **41**, 434–445.
6 W. V. Graham, A. Bonito-Oliva and T. P. Sakmar, *Annu. Rev. Med.*, 2017, **68**, 413–430.
7 F. Prati, G. Bottegoni, M. L. Bolognesi and A. Cavalli, *J. Med. Chem.*, 2018, **61**, 619–637.
8 J. F. Gonzalez, A. R. Alcantara, A. L. Doadrio and J. M. Sanchez-Montero, *Expert Opin. Drug Discovery*, 2019, **14**, 879–891.
9 T. Storr, *Can. J. Chem.*, 2021, **99**, 1–9.
10 S. Samanta, K. Rajasekhar, M. Ramesh, N. A. Murugan, S. Alam, D. Shah, J. P. Clement and T. Govindaraju, *Adv. Ther.*, 2021, **4**, 2000225.
11 M. Ramesh, C. Balachandra, P. Andhare and T. Govindaraju, *ACS Chem. Neurosci.*, 2022, **13**, 2209–2221.
12 J. M. Tarasoff-Conway, R. O. Carare, R. S. Osorio, L. Glodzik, T. Butler, E. Fieremans, L. Axel, H. Rusinek, C. Nicholson, B. V. Zlokovic, B. Frangione, K. Blennow, J. Menard, H. Zetterberg, T. Wisniewski and M. J. de Leon, *Nat. Rev. Neurol.*, 2015, **11**, 457–470.
13 T. E. Golde, *J. Neurochem.*, 2016, **139**(suppl 2), 224–236.
14 D. W. Choi, *Neurosci. Lett.*, 1985, **58**, 293–297.
15 S. Agarwal, R. K. Tannenberg and P. R. Dodd, *J. Alzheimer's Dis.*, 2008, **14**, 313–321.
16 R. Wang and P. H. Reddy, *J. Alzheimer's Dis.*, 2017, **57**, 1041–1048.
17 A. Aliyan, N. P. Cook and A. A. Martí, *Chem. Rev.*, 2019, **119**, 11819–11856.
18 Y. W. Jun, S. W. Cho, J. Jung, Y. Huh, Y. Kim, D. Kim and K. H. Ahn, *ACS Cent. Sci.*, 2019, **5**, 209–217.
19 H. Arora, M. Ramesh, K. Rajasekhar and T. Govindaraju, *Bull. Chem. Soc. Jpn.*, 2020, **93**, 507–546.
20 K. Rajasekhar, N. Narayanaswamy, N. A. Murugan, K. Viccaro, H.-G. Lee, K. Shah and T. Govindaraju, *Biosens. Bioelectron.*, 2017, **98**, 54–61.
21 H. Yang, F. Zeng, Y. Luo, C. Zheng, C. Ran and J. Yang, *Molecules*, 2022, **27**, 3879.
22 J. Yang, Y. Guo, M. Pistolozzi and J. Yan, *Dyes Pigm.*, 2021, **193**, 109466.
23 M. Ramesh and T. Govindaraju, *Chem. Sci.*, 2022, **13**, 13657–13689.
24 W. Yang, Y. Wong, O. T. Ng, L. P. Bai, D. W. Kwong, Y. Ke, Z. H. Jiang, H. W. Li, K. K. Yung and M. S. Wong, *Angew. Chem., Int. Ed.*, 2012, **51**, 1804–1810.
25 Y. Li, D. Xu, S. L. Ho, H. W. Li, R. Yang and M. S. Wong, *Biomaterials*, 2016, **94**, 84–92.
26 Y. Li, D. Xu, A. Sun, S. L. Ho, C. Y. Poon, H. N. Chan, O. T. W. Ng, K. K. L. Yung, H. Yan, H. W. Li and M. S. Wong, *Chem. Sci.*, 2017, **8**, 8279–8284.
27 X. Wang, C. Wang, H.-N. Chan, I. Ashok, S. K. Krishnamoorthi, M. Li, H. W. Li and M. S. Wong, *Talanta*, 2021, **224**, 121830.
28 Y. Li, C. Chen, D. Xu, C. Y. Poon, S. L. Ho, R. Zheng, Q. Liu, G. Song, H. W. Li and M. S. Wong, *ACS Omega*, 2018, **3**, 6812–6819.

29 C. Chen, D. Xu, Z.-H. Zhang, S.-Z. Jia, X.-C. Cao, Y.-B. Chen, G.-L. Song, M. S. Wong and H. W. Li, *Exp. Neurol.*, 2020, **327**, 113210.
30 K. Rajasekhar, N. Narayanaswamy, N. A. Murugan, G. Kuang, H. Ågren and T. Govindaraju, *Sci. Rep.*, 2016, **6**, 23668.
31 G. E. Hardingham and H. Bading, *Nat. Rev. Neurosci.*, 2010, **11**, 682–696.
32 G. E. Hardingham, Y. Fukunaga and H. Bading, *Nat. Neurosci.*, 2002, **5**, 405–414.
33 M. Talantova, S. Sanz-Blasco, X. Zhang, P. Xia, M. W. Akhtar, S. Okamoto, G. Dziewczapolski, T. Nakamura, G. Cao, A. E. Pratt, Y. J. Kang, S. Tu, E. Molokanova, S. R. McKercher, S. A. Hires, H. Sason, D. G. Stouffer, M. W. Buczynski, J. P. Solomon, S. Michael, E. T. Powers, J. W. Kelly, A. Roberts, G. Tong, T. Fang-Newmeyer, J. Parker, E. A. Holland, D. Zhang, N. Nakanishi, H. S. Chen, H. Wolosker, Y. Wang, L. H. Parsons, R. Ambasudhan, E. Masliah, S. F. Heinemann, J. C. Pina-Crespo and S. A. Lipton, *Proc. Natl. Acad. Sci. U. S. A.*, 2013, **110**, E2518–2527.
34 X. Wang, H.-N. Chan, N. Desbois, C. Gros, F. Bolze, Y. Li, H. W. Li and M. S. Wong, *ACS Appl. Mater. Interfaces*, 2021, **13**(16), 18525–18532.